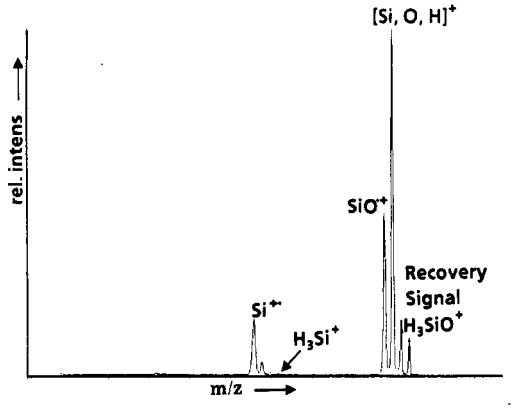

Figure 13. $^{-}NR^{+}$ spectrum of $[Si,O,H_3]^+$ generated from $[Si,O,H_3]^-$ via CR (O_2, 80% T; O_2, 80% T).

is practically identical to the CR spectrum shown in Figure 12 and contains a fairly intense recovery signal (although again not sufficiently large for further CA). We take this as evidence for the intermediate formation of a neutral molecule with the connectivity $H_3SiO^{\bullet}$.

IV. Conclusions

1. Collisional activation experiments have established the connectivities $HSiOH^+$ and H_2SiOH^+ for the ions at m/z 46 and 47 generated by electron impact of tetramethoxysilane.

2. Neutralization–reionization experiments have established the connectivities HSiOH and $H_2SiOH^{\bullet}$ for the neutral species derived from $HSiOH^{\bullet+}$ and H_2SiOH^+ by neutralization at high collision energies. The connectivity for HSiOH is the same as that predicted by theory for the ground state of this molecule.

3. Charge-reversal experiments with $H_2SiO^{\bullet-}$ and H_3SiO^- have established the connectivities $H_2SiO^{\bullet+}$ and H_3SiO^+. Theoretical predictions suggest that the H_3SiO^+ ion produced by charge reversal of the siloxide anion is the higher energy isomer and that this ion must be in its triplet state.

4. Neutralization–reionization experiments have provided evidence for the stability of the neutral molecules H_2SiO and $H_3SiO^{\bullet}$.

Acknowledgment. Financial support of our work by the Deutsche Forschungsgemeinschaft and the Fonds der Chemischen Industrie is appreciated. R.S. acknowledges the receipt of a visiting fellowship from the Deutscher Akademischer Austauschdienst (DAAD) and the encouragement of Dr. A. V. Rama Rao, Director, IICT, Hyderabad (India). D.K.B. is grateful to the Alexander-von-Humboldt Foundation for a Humboldt Senior Scientist Award and to Professor H. Schwarz for his hospitality. We are indebted to Dr. Thomas Weiske for technical assistance.

Reaction Kinetics of Coordinatively Unsaturated Iron Carbonyls Formed on Gas-Phase Excimer Laser Photolysis of $Fe(CO)_5$

Robert J. Ryther and Eric Weitz*

Department of Chemistry, Northwestern University, Evanston, Illinois 60208-3113
(Received: December 27, 1990; In Final Form: July 8, 1991)

The reactions of species produced on gas-phase excimer laser photolysis of $Fe(CO)_5$ have been followed by transient infrared spectroscopy employing a diode laser probe. The initial photoproducts formed on 193-nm photolysis are identified as $Fe(CO)_2$ and a product that is most likely Fe(CO). Both $Fe(CO)_2$ and $Fe(CO)_3$ are produced on 248-nm photolysis. Photolysis at 351 nm leads to the production of both $Fe(CO)_3$ and $Fe(CO)_4$. Species best assigned as excited states of $Fe(CO)_3$ and $Fe(CO)_4$ are observed to form as initial photoproducts following 248- and 351-nm photolysis, respectively. The magnitudes of the rate constants for reaction of the various coordinatively unsaturated metal carbonyls formed in this study with parent $Fe(CO)_5$ or CO (summarized in Table I) are consistent with the hypothesis that spin-allowed reactions will be rapid while spin-disallowed reactions will be considerably slower. To provide further data in testing this hypothesis, the reaction of $Fe(CO)_4$ with both O_2 and H_2 has been measured.

I. Introduction

Studies of metal carbonyl photochemistry have provided a wealth of information on the photochemistry, photophysics, and reactive behavior of coordinatively unsaturated species.[1-15] A particularly well-studied and important metal carbonyl is $Fe(CO)_5$. It has been shown that photolysis of $Fe(CO)_5$ can lead to the production of active catalytic species for olefin hydrogenation,[1-3] hydrosilation,[4-7] and isomerization[2,3,8,9] reactions. Gas-phase, UV photolysis of $Fe(CO)_5$ has been used for deposition of thin films of metal on semiconductor or magnetic memory storage devices[10,11] and for deposition of iron carbonyl catalysts on surfaces.[5-7,12,13] Similarities between metal carbonyls and carbon monoxide bound to metal surfaces also aid in modeling of surface–molecule interactions[12] which can be used in interpreting both theoretical and experimental surface science studies.

Applications of transient infrared spectroscopy to the study of coordinatively unsaturated metal carbonyls is relatively recent, but it is already clear that this technique has revealed a number of new and interesting features regarding the photochemistry and reactive behavior of these species.[15] Though almost all the coordinatively unsaturated metal carbonyls that have been studied to date react very rapidly with CO and the parent carbonyl, $Fe(CO)_4$ is an anomaly. Its rate constant for reaction with CO

(1) Whetten, R. L.; Fu, K. J.; Grant, E. R. *J. Chem. Phys.* **1982**, *77*, 3769.
(2) Wrighton, M. S.; Ginley, D. S.; Schroeder, M. A.; Morse, D. L. *Pure Appl. Chem.* **1975**, *41*, 671.
(3) Schroeder, M. A.; Wrighton, M. S. *J. Am. Chem. Soc.* **1976**, *98*, 551.
(4) Mitchener, J. C.; Wrighton, M. S. *J. Am. Chem. Soc.* **1981**, *103*, 975.
(5) Trusheim, M R.; Jackson, R. L. *J. Phys. Chem.* **1983**, *87*, 1910.
(6) Jackson, R. L.; Trusheim, M. R. *J. Am. Chem. Soc.* **1982**, *104*, 6590.
(7) Darsillo, M. S.; Gafney, H. D.; Paquette, M. S. *J. Am. Chem. Soc.* **1987**, *109*, 3275.
(8) Whetten, R. L.; Fu, K. J.; Grant, E. R. *J. Am. Chem. Soc.* **1982**, *104*, 4270.
(9) Weiller, B. H.; Grant, E. R. *J. Am. Chem. Soc.* **1987**, *109*, 1051.
(10) Kompa, K. L. *Angew. Chem., Int. Ed. Engl.* **1988**, *27*, 1314.
(11) Schröder, H.; Kompa, K. L.; Masci, D.; Gianinoni, I. *Appl. Phys.* **1985**, *A38*, 227.
(12) Plummer, E. W.; Salaneck, W. R.; Miller, J. S. *Phys. Rev. B* **1978**, *18*, 1673.
(13) Swanson, J. R.; Friend, C. M.; Chabal, Y. J. *J. Chem. Phys.* **1987**, *87*, 5028.
(14) Barton, T. J.; Grinter, R.; Thomson, A. J.; Davies, B.; Poliakoff, M. *J. Chem. Soc., Chem. Commun.* **1977**, 841.
(15) Poliakoff, M.; Weitz, E. *Adv. Organometallic Chem.* **1986**, *25*, 277. *Acc. Chem. Res.* **1987**, *20*, 408.

0022-3654/91/2095-9841$02.50/0

is approximately 400 times smaller than the rate constant for the corresponding process for $Fe(CO)_3$. This behavior has been explained as due to the spin-forbidden nature of the reaction of $Fe(CO)_4 + CO$ to generate $Fe(CO)_5$.[15] $Fe(CO)_4$ has been shown to be paramagnetic[14] and has a triplet ground state while $Fe(CO)_5$ has a singlet ground state.

This study focuses on product distributions and reactions of coordinatively unsaturated iron carbonyls that are produced on excimer laser photolysis of $Fe(CO)_5$. The use of a continuous wave, continuously tunable IR diode laser in place of a CO laser as a probe of the transient iron carbonyls extends both the frequency range that can be studied as well as the time range, due to the increased long time scale stability of a diode laser versus the CO laser. Both of these factors are important for monitoring kinetic processes that lead to the production of polynuclear iron reaction products. In addition, since the diode laser can be tuned to any arbitrary frequency, it is not affected by the production of vibrationally excited CO on photolysis of $Fe(CO)_5$. Excited CO necessarily absorbs the CO probe laser, thus obscuring metal carbonyl absorptions in the same spectral region as the vibrationally excited or even ground-state CO molecules. This is not a problem with the diode laser, which allows for a more detailed investigation of the product distributions and their reactive behavior than was previously possible with a CO laser probe. The CO laser's spectral range is also limited ($\sim$2050–$\sim$1600 cm^{-1}) in comparison with the IR diode laser, where diodes are available which span virtually the entire infrared spectrum. As some of the strongest absorptions of the dinuclear iron carbonyls are found above 2050 cm^{-1}, the IR diode laser is an excellent probe of these species in a time-resolved infrared spectroscopy (TRIS) experiment.

This investigation presents a study of the reactions of the photoproducts produced on the single-photon photolysis of $Fe(CO)_5$ at 193, 248, and 351 nm. Additional information is available from the diode laser probe which impacts on previous assignments of photoproducts. The rate constants for the reaction of photofragments with $Fe(CO)_5$ are reported for the first time as are the pathways and rate constants for a number of reactions involving polynuclear iron species. Of particular interest is the influence the reactant and product spin states have on the rates and pathways for these reactions.

II. Experimental Section

The TRIS apparatus is shown schematically in Figure 1. The experimental details are similar to those described previously;[15] however, a brief description will be provided for convenience. In a typical experiment sample gases are passed through mass flow controllers (MKS, Tylan) into a 35 cm × 1.5 cm diameter flow cell fitted with CaF_2 windows. The cell is equipped with ports at both ends that permit purging of the windows with rare gas to prevent the deposition of UV- and IR-absorbing photoproducts. Flow rates and pressures are adjusted so that the purge gases do not mix with the samples gases. Gases are replenished before the next UV pulse at a rate of 1 Hz. $Fe(CO)_5$ is photolyzed by using the pulsed, unfocused output of an excimer laser (Questek 2200 series) running on ArF (193 nm), KrF (248 nm), and XeF (351 nm). The UV beam completely fills the cell in order to create a spatially uniform product concentration. The UV laser fluences were measured by using a Scientec power meter to be approximately 3 mJ/cm^2 for ArF and 10 mJ/cm^2 for KrF and XeF excimer laser pulses. These fluences are well below the limit where two photon processes are significant as determined by Hepburn and co-workers.[16,17] Indeed, our photoproduct signal amplitudes were observed to vary linearly with the UV laser fluence, which is consistent with a single-photon process.

The IR probe is a tunable diode laser (Laser Analytics SP5800) which is collimated, passed through a 0.5-m monochromator (f/11 Czerney-Turner), double passed through the center of the flow

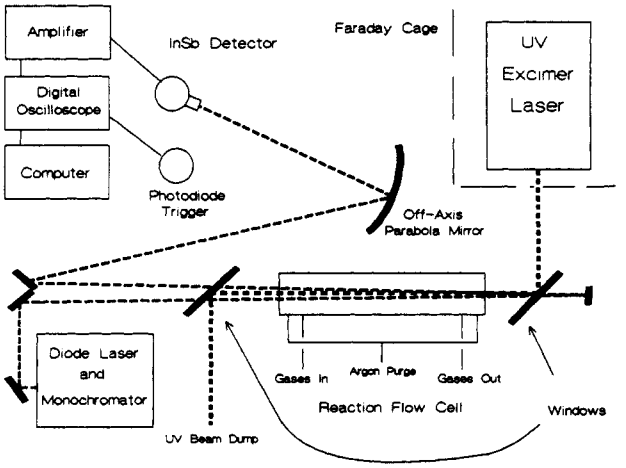

Figure 1. A schematic of the time-resolved infrared spectroscopy apparatus.

cell, and focused on a liquid nitrogen cooled InSb photovoltaic detector (SBRC). The detector output is amplified (Perry, 100×), then digitized and averaged by using a Lecroy 9400 digital oscilloscope, and stored on an IBM-AT computer for analysis. The $1/e$ rise time of the InSb detector used in this study and its associated electronics was measured experimentally to be $\sim$60 ns. Pressures were measured by a MKS capacitance manometer.

Coordinatively unsaturated photoproducts of the UV photolysis of $Fe(CO)_5$ are detected by monitoring the attenuation of the IR probe beam over a variable time range from the 60-ns detector response time to, in some cases, as long as approximately 50 ms. Time-resolved IR spectra are obtained by first collecting transient wave forms at a uniform resolution (usually 2 or 4 cm^{-1}) over the iron carbonyl CO stretching region. Points are taken from the transients at different wavelengths at a common delay time and are connected to produce a spectrum of the system at that delay time. The single-time spectra may then be incremented at regular intervals, resulting in a time-resolved spectrum which permits one to observe relative changes in absorbance of parent and transient species. A positive change in absorbance in the spectra presented in this paper represents product formation.

The IR diode laser, with a resolution in the range of 10^{-4} cm^{-1}, is typically used as a high-resolution probe of vibration–rotation spectra of molecules. In this study it is employed in the more unusual application of probing the continuous, broad-band absorptions of iron carbonyl photofragments and reaction products over approximately 200 wavenumbers. The continuous absorptions of iron carbonyls at room temperature result from a high density of low-lying vibrational modes possibly acting in concert with a fluxional structure. Rotational splitting of $Fe(CO)_5$ has so far only been observed at the very low temperatures achieved in a supersonic free jet.[18] Because of the lack of rotational resolution in the species of interest, an extremely tedious search for rotational maxima at each spectral point is avoided. Therefore, the transient IR spectra obtained with a diode laser provides a true representation of the infrared spectra of individual transient and product molecules.

Kinetic information was obtained by monitoring the change in rate of a single-frequency transient signal with varying amounts of reactive gas [$Fe(CO)_5$, CO, H_2 and O_2], which is normally present in large excess. All reported rate constants were obtained at room temperature (295 ± 1 K). Signals were fit by using the Provencher multiexponential fitting routine.[19]

Activation energies were probed by varying the temperature of the experimental cell as well as the gas inlet tubing over a range from 295 to 415 K [the temperature at which $Fe(CO)_5$ exhibited significant decomposition in our cell] using heating tape. The cell and the inlet tubing were insulated with glass wool. Thermal equilibrium of the gases was verified by monitoring the temper-

(16) Waller, I. M.; Davis, H. F.; Hepburn, J. W. *J. Phys. Chem.* **1987**, *91*, 506.
(17) Waller, I. M.; Hepburn, J. W. *J. Chem. Phys.* **1988**, *88*, 6658.
(18) Matsumoto, Y.; Majima, T.; Takami, M. *Mol. Phys.*, **1987**, *61*, 1045.
(19) Provencher, S. W. *Biophys. J.* **1976**, *16*, 27.

ature with thermocouples placed in contact with the gas in the center and at the ends of the cell.

The $Fe(CO)_5$ used in this study was obtained from Alfa Products and degassed by successive freeze–pump–thaw cycles. It was then vacuum transferred to a trap filled with glass beads and kept in the dark. This sample was degassed prior to each experiment and then frozen by using a constant-temperature ethanol refrigerator at a temperature such that the vapor pressure of the solid was approximately 20% higher than the maximum pressure of $Fe(CO)_5$ desired for a particular experiment. Argon (Matheson, 99.995% purity) or CO (Matheson, 99.995%) act as an iron pentacarbonyl carrier gas. The flow of the carrier gas was first regulated by a mass flow controller and subsequently passed through the trap containing $Fe(CO)_5$ frozen on glass beads. The $Fe(CO)_5$/carrier gas was mixed with other system gases prior to reaching the reaction cell. When H_2 (Matheson, 99.999%) and O_2 (Linde, 99.6%) were used as reactant gases, argon was employed as the carrier gas.

The $Fe(CO)_5$ concentration was determined for each flow setting by using a diode laser to probe the absorbance of the contents of the flow cell at a wavelength where there is a well-known absorption coefficient for $Fe(CO)_5$. $Fe(CO)_5$ pressures used for the time-resolved spectra were 12.5 mTorr for 193 nm, 10 mTorr for 248 nm, and 80 mTorr for 351 nm. An argon buffer gas was used in most experiments in order to increase the heat capacity of the system which serves to damp shock waves that can result from inhomogeneous deposition of photolysis energy or release of energy by relaxation and/or reaction of photoproducts. It also acts as a third body for association reactions.

III. Results and Discussion

A. 193-nm Photolysis of $Fe(CO)_5$. 1. Initial Photoproducts. Figure 2 depicts time-resolved spectra generated following photolysis of $Fe(CO)_5$ with 193-nm radiation. Figure 2A is a spectrum showing the time evolution of the system over the first 1.0 μs at 0.1 μs/interval. Feature 5 is due to depletion of $Fe(CO)_5$ on photolysis (negative change in absorbance), while two distinct photoproducts are produced (positive absorptions). The photoproduct at ~1920 cm^{-1}, labeled as feature 2, was assigned by Weitz and co-workers[20] as $Fe(CO)_2$. The assignment of $Fe(CO)_2$ was made in ref 20 by using the "kinetic bootstrap" method by which sequential reactions of an $Fe(CO)_2$ photofragment with CO were followed in real time until parent $Fe(CO)_5$ was eventually reformed. Studies by Vernon and co-workers[21,22] and Hepburn and co-workers[16,17] are in agreement that $Fe(CO)_2$ is the major product produced on 193-nm photolysis of $Fe(CO)_5$. The absorption at 1950 cm^{-1} (feature 1) was not definitively assigned in ref 20. However, possible assignments were discussed including Fe(CO) and an excited state of $Fe(CO)_3$.

The current study, unlike the study of ref 20, which was performed with a CO laser probe, is unaffected by vibrationally excited CO in the region of feature 1 and reveals more detail about this absorption. From Figure 2A it can be seen that $Fe(CO)_2$ has a signficant amount of vibrational excitation evidenced by the narrowing and shifting of its absorption band (feature 2) to higher frequencies as $Fe(CO)_2$ is collisionally relaxed.[23] As feature 1 does not exhibit any observable vibrational excitation, the most plausible assignment for this species is either the more highly unsaturated iron carbonyl, Fe(CO), or an electronically excited photofragment such as a singlet state of $Fe(CO)_3$ or $Fe(CO)_2$. Since there is no change in the amplitude of feature 1 for a spectrum taken with 10 Torr of argon (the conditions used in the spectra in Figure 2) or 80 Torr of Ar, it is unlikely that feature 1 is due to a highly excited $Fe(CO)_3$ photofragment which is

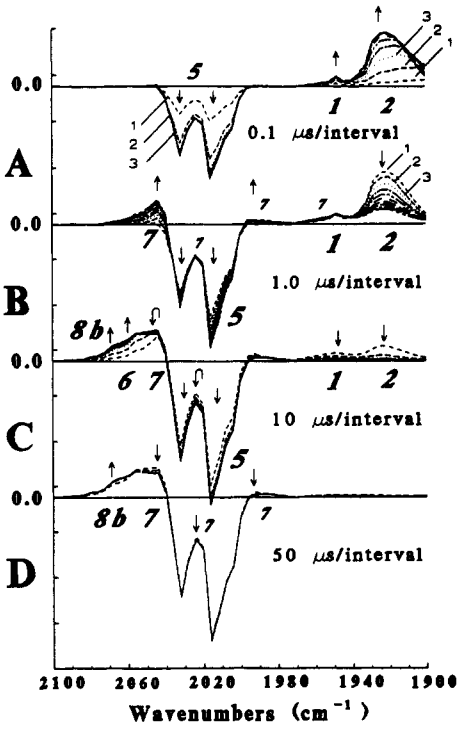

Figure 2. Time-resolved spectra generated upon 193-nm photolysis of $Fe(CO)_5$ for a sample containing 10 mTorr of $Fe(CO)_5$ and 10 Torr of argon buffer gas. Panels A–C are segmented into 10 equal time intervals with ranges of (A) 1.0 μs, (B) 10.0 μs, and (C) 100.0 μs. Panel D is segmented into 4 equal time intervals over a range of 200 μs. The ordinate is in arbitrary absorbance units with the zero of absorbance indicated. In panels A and B the first three traces are labeled. Arrows indicate the direction of change of various features during the indicated time intervals. See text for assignments.

collisionally stabilized before it can dissociate to form the $Fe(CO)_2$ species.[20]

Feature 1 in Figure 2A also does not behave as has been observed for other excited electronic states produced on $Fe(CO)_5$ photolysis. As will be discussed in more detail in subsequent sections, following 248- and 351-nm photolysis of $Fe(CO)_5$, initial photoproducts are observed that are best assigned as excited electronic states of $Fe(CO)_3$ and $Fe(CO)_4$ (discussed in sections B and C below). In contrast to feature 1, these species are readily collisionally quenched to their respective ground states by rare gas collisions whereas, as previously stated, feature 1 is not affected by changes in rare gas pressure.

Despite this behavior, the possibility that feature 1 in Figure 2A is a stable electronically excited species cannot be completely disregarded, but an assignment to an excited electronic state of $Fe(CO)_2$ is also unlikely due to energy considerations. The lowest electronically excited state of $Fe(CO)_2$ was calculated by Guenzburger et al. to be 2.4 eV above the ground state.[24] Since the sum of the bond dissociation energies for three CO ligands ejected on formation of the ground state of $Fe(CO)_2$ is reported to be approximately 4.0 eV,[25] the energy necessary to produce the first electronically excited singlet state of $Fe(CO)_2$ is ~6.4 eV above ground state $Fe(CO)_5$. Although this energy is comparable to the 6.42 eV energy of a 193-nm photon, formation of this singlet excited state of $Fe(CO)_2$ would require the three ejected CO ligands to form with essentially no excess energy. Formation of "cold" photoejected CO is contrary to the observations of Hepburn and co-workers who measured an average of 0.6 eV removed by each CO ligand on 193-nm photolysis of $Fe(CO)_5$.[17] Therefore, it is unlikely that the excited singlet state of $Fe(CO)_2$ is formed in any significant quantity. Although, on the basis of

(20) Seder, T. S.; Ouderkirk, A. J.; Weitz, E. *J. Chem. Phys.* **1986**, *85*, 1977.
(21) Ray, U.; Brandow, S. L.; Bandukwalla, G.; Venkataraman, B. K.; Zhang, Z.; Vernon, M. *J. Chem. Phys.* **1988**, *89*, 4092.
(22) Venkataraman, B. K.; Bandukwalla, G.; Zhang, Z.; Vernon, M. *J. Chem. Phys.* **1989**, *90*, 5510.
(23) Ouderkirk, A. J.; Seder, T. A.; Weitz, E. *Proc. SPIE—Int. Soc. Opt. Eng.* **1984**, *458*, 148.
(24) Guenzburger, D.; Saitovitch, E. M. B.; DePaoli, M. A.; Manela, H. *J. Chem. Phys.* **1984**, *80*, 735.
(25) Engelking, P. C.; Lineberger, W. C. *J. Am. Chem. Soc.* **1979**, *101*, 5569.

the data in ref 23, an electonically excited state of $Fe(CO)_3$ is energetically possible, such a species would differ from the electronically excited state of $Fe(CO)_3$ that is observed following 248-nm photolysis (vide infra). Further, as previously stated, this species would also have to be collisionally metastable.

The energy required to form ground-state Fe(CO) is calculated to be approximately 5 eV.[24] An average energy disposal of ~0.4 eV to each of the four CO ligands would permit the formation of Fe(CO) with a 193-nm photon. Although this degree of CO excitation is smaller than that measured by Hepburn, bond dissociation energies are known at best to ±0.3 eV. The magnitude of the errors in the bond dissociation energy easily provides for enough energy to produce Fe(CO) and internally excited CO.

Hepburn calculates the formation of approximately 1% Fe(CO) in his molecular beam study on the basis of Fe(CO) formation from the high-energy tail of the $Fe(CO)_2$ distribution.[17] Such a distribution would be expected to be broadened in our room temperature study due to the additional thermal energy of the $Fe(CO)_5$ parent. This could result in formation of additional Fe(CO) following 193-nm photolysis of a room temperature sample of $Fe(CO)_5$. As discussed in ref 26, the Fe(CO) produced on room temperature photolysis represents ~10% of the total product formed on 193-nm photolysis of $Fe(CO)_5$.

Although Vernon and co-workers do not report formation of Fe(CO) in their 193-nm photolysis of $Fe(CO)_5$ in a molecular beam,[22] it is not clear to us from the discussion in that study whether, at the level we observe or the reduced level that might be expected in a beam, Fe(CO) could be distinguished, via their time-of-flight technique, from the only observed product, $Fe(CO)_2$.

Yardley and co-workers[27] did report formation of Fe(CO) in their study of the 193-nm photolysis of $Fe(CO)_5$. However, there are significant differences in the product distributions measured by Yardley et al. for 193-, 248-, and 351-nm $Fe(CO)_5$ photolysis and the results reported in this study and in ref 20. Thus agreement on the production of Fe(CO) following 193-nm photolysis should be regarded with caution.

Unfortunately, it was not possible to confirm the Fe(CO) assignment by the "kinetic bootstrap" procedure used for assignments in ref 20 due to the large amounts of $Fe(CO)_2$ present. The reaction of $Fe(CO)_2$ with added CO produces large amounts of $Fe(CO)_3$ whose absorption overlaps that of feature 1, thus obscuring its behavior. Additionally, since $Fe(CO)_2$ is being rapidly depleted due to its reaction with CO, and since a relatively small amount of Fe(CO) is present, it is not possible to definitively determine if the product of the reaction of Fe(CO) + CO is $Fe(CO)_2$, as would be expected. Nevertheless, we feel the best assignment of the absorption labeled feature 1 in Figure 2 is to Fe(CO).

The Fe(CO) absorption reverses the trend that more saturated iron carbonyl species absorb at higher frequencies (see iron carbonyl absorption frequencies in Table I). This same behavior is reported by Pearson and co-workers, who reported IR spectra of Fe(CO) and $Fe(CO)_2$ in a low-temperature rare gas matrix.[28] Although the spectral shifts from the matrix to the gas phase are abnormally large (on the order of 50 cm^{-1} versus the more typical shifts of ~5–~20 cm^{-1}), the difference in frequency between the Fe(CO) and the $Fe(CO)_2$ species and the relative positions observed in Pearson's study are compatible with our observations. Similar behavior was observed in the gas-phase TRIS study of $Cr(CO)_6$ photolysis: $Cr(CO)_2$ absorbs at a higher frequency than $Cr(CO)_3$.[29] This reversal of the more common situation, where $M(CO)_x$ absorbs at a higher frequency than $M(CO)_{x-1}$, can be rationalized by consideration of the possible magnitude of energy-factored force constants and interaction constants for unsaturated metal carbonyls. Timney has shown that these constants can span a fairly wide range of values for different metals and different values of x.[30]

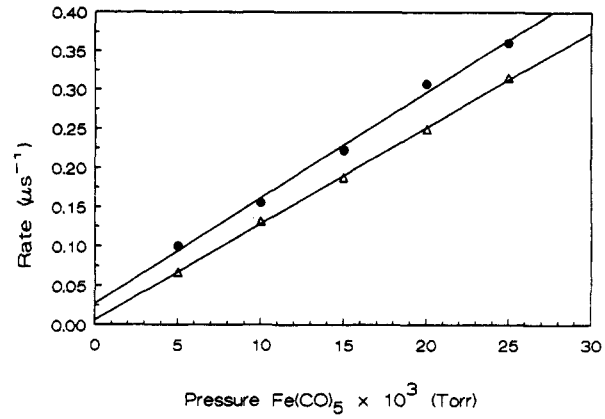

Figure 3. A plot of the pseudo-first-order rate constant for the reaction of $Fe(CO)_2$ + $Fe(CO)_5$. The rate of decay of $Fe(CO)_2$ at 1912 cm^{-1} (●) and the rate of formation of $Fe_2(CO)_7$ at 2044 cm^{-1} (△) are plotted against the pressure of $Fe(CO)_5$. The average slope of the linear least-squares fits gives a rate constant of 12 ± 1.8 μs^{-1} $Torr^{-1}$ or (3.7 ± 0.6) × 10^{-10} cm^3 $molecule^{-1}$ s^{-1}.

2. Reactions of Photoproducts following 193-nm Photolysis. Figure 2B illustrates the further time evolution of the iron carbonyl photofragments on a 10-μs time scale. The decay of $Fe(CO)_2$ (feature 2 in Figure 2B) and the matching secondary decay (following the initial loss in amplitude due to photolysis) of $Fe(CO)_5$ (feature 5 in Figure 2B) indicate a reaction of $Fe(CO)_2$ with parent. The dinuclear product from that reaction has absorptions at 2045, 2025, 2000 and 1950 cm^{-1} (marked as feature 7 in Figure 2B). In Figure 3, the decay rate of $Fe(CO)_2$ and the rise rate of the dinuclear product monitored at 2045 cm^{-1} are plotted for a range of parent pressures. The slope is the rate constant for the reaction that produces dinuclear product and is 12 (±1.8) μs^{-1} $Torr^{-1}$ [(3.7 ± 0.6) × 10^{-10} cm^3 $molecule^{-1}$ s^{-1}] for both sets of data. This rate constant is of similar magnitude to a gas kinetic rate constant which for this system is expected to be approximately 5 × 10^{-10} cm^3 $molecule^{-1}$ s^{-1}.

Feature 7 is most likely a previously unreported $Fe_2(CO)_7$ species. Though it is possible that CO loss from the dinuclear product occurs as part of the association reaction, the association reactions of $Fe(CO)_3$ and $Fe(CO)_4$ with parent produce products that correlate much better with association reactions that occur with retention of all CO's rather than with an association reaction and subsequent or simultaneous decarbonylation. The primary example is that of formation of $Fe_2(CO)_9$ in the 351-nm photolysis to be discussed in detail in section III.C.2 below. The same $Fe_2(CO)_9$ species is observed to form through two distinct pathways on 351-nm photolysis, the first being the reaction of $Fe(CO)_4$ + $Fe(CO)_5$ and the second being the reaction of the unbridged $Fe_2(CO)_8$ isomer with CO. In addition, as discussed below, CO addition to the species assigned as $Fe_2(CO)_7$ yields a product whose absorptions correlate well with an isomer of $Fe_2(CO)_8$ previously seen in a matrix environment. This $Fe_2(CO)_7$ species absorbs at the same frequencies and demonstrates the same kinetic behavior as the dinuclear species formed on reaction of $Fe(CO)_2$ with parent following 248-nm photolysis of $Fe(CO)_5$ (vide infra).

Figure 2B demonstrates that under experimental conditions $Fe(CO)_2$ reacts significantly before reaction of Fe(CO) is evident. In Figure 2C, which is on a 100-μs time scale, Fe(CO) (feature 1) decay is evident as the parent decay continues. Another dinuclear product grows in and is labeled feature 6 in Figure 2C. The kinetic data in Figure 4 demonstrate that the reaction of Fe(CO) + $Fe(CO)_5$ produces feature 6. The rise rate of the dinuclear product and the fall rate of Fe(CO) are plotted as a function of $Fe(CO)_5$ pressure, and both sets of data give a rate constant for this reaction of 2.8 (±0.8) μs^{-1} $Torr^{-1}$ [(8.6 ± 2.5) × 10^{-11} cm^3 $molecule^{-1}$ s^{-1}]. No change in reaction rate was

(26) Ryther, R. J.; Weitz, E. To be published.
(27) Yardley, J. T.; Gitlin, B.; Nathanson, G.; Rosan, A. M. *J. Chem. Phys.* **1981**, *74*, 370.
(28) Peden, C. H. F.; Parker, S. F.; Barrett, P. H.; Pearson, R. G. *J. Chem. Phys.* **1983**, *87*, 2329.
(29) Seder, T. A.; Church, S. P.; Ouderkirk, A. J.; Weitz, E. *J. Am. Chem. Soc.* **1985**, *107*, 1432.
(30) Timney, J. A. *Inorg. Chem.* **1979**, *18*, 2502.

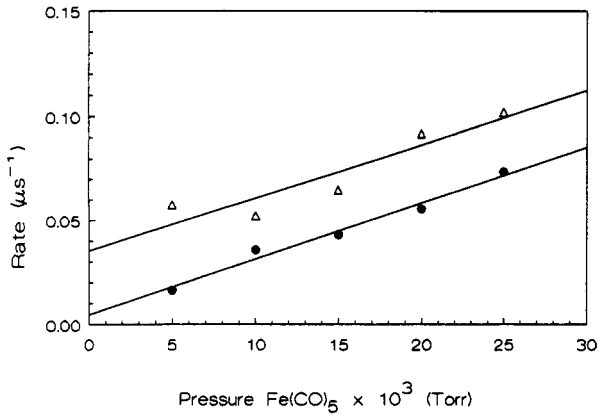

Figure 4. A plot of the pseudo-first-order rate constant for the reaction of Fe(CO) + $Fe(CO)_5$. The rate of decay of Fe(CO) at 1956 cm^{-1} (△) and the rate of formation of $Fe_2(CO)_6$ at 2064 cm^{-1} (●) are plotted against the pressure of $Fe(CO)_5$. The average slope of the linear least-squares fits gives a rate constant of 2.8 ± 0.8 μs^{-1} $Torr^{-1}$ or (8.6 ± 2.5) × 10^{-11} cm^3 $molecule^{-1}$ s^{-1}.

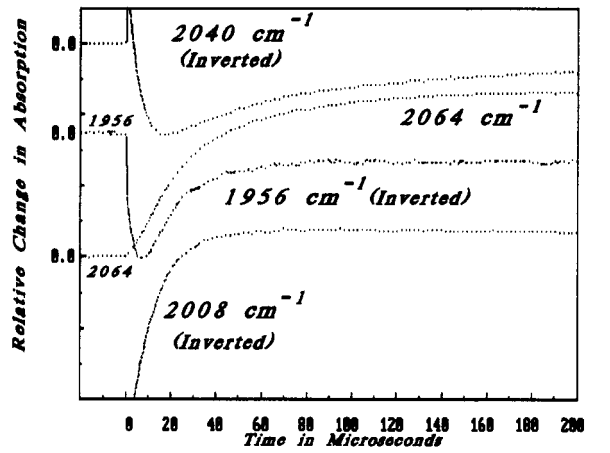

Figure 5. A plot of four single-frequency time-resolved signals generated on 193-nm photolysis of $Fe(CO)_5$. The 2040, 2008, and 1956-cm^{-1} signals are shown inverted. See text for assignments and discussion.

observed on changing the buffer gas pressure from 10 to 80 Torr of argon, indicating that the rate constant represents the microscopic rate constant for the association step in this reaction.[20]

The absorption designated as feature 6 differs in frequency from the absorptions observed for the two isomers of $Fe_2(CO)_8$ that result from the reactions of $Fe(CO)_3$ + $Fe(CO)_5$ (see section III.C) and $Fe_2(CO)_7$ + CO (discussed below). It also differs from the $Fe_2(CO)_7$ isomer formed by reaction of ground-state $Fe(CO)_2$ + $Fe(CO)_5$ observed following both the 193-nm and the 248-nm photolysis of $Fe(CO)_5$. Feature 6 is tentatively assigned to $Fe_2(CO)_6$ produced by the reaction of Fe(CO) + $Fe(CO)_5$. This assignment is based on the assumption of retention of all CO's by the dinuclear product as occurs with the other dinuclear products observed in this study.

No further reaction with $Fe(CO)_5$ is observed after the decay of Fe(CO), yet Figure 2D demonstrates that there is an observable reaction of the $Fe_2(CO)_7$ species taking place over a 200-μs time scale. It is apparent that $Fe_2(CO)_7$ is reacting to produce feature 8b in Figure 2D. Figure 5 displays the single-frequency time-resolved IR signals taken at 2064, 2040, 2008, and 1956 cm^{-1}, demonstrating the agreement between the decay rate of $Fe_2(CO)_7$ at 2040 cm^{-1} (shown in Figure 5) and the rise of feature 8b at 2064 cm^{-1}. Figure 5 also clearly demonstrates that no change in the parent concentration (2008 cm^{-1}) occurs on the time scale of these signals. The lack of parent decay on the timescale of this rise suggests that $Fe_2(CO)_7$ reacts with CO formed on photolysis of $Fe(CO)_5$. [Fe(CO) at 1956 cm^{-1} is also shown to have completed its decay well before the product growing in at 2064 cm^{-1} completes its formation.] With the 193-nm photon flux used for this study, approximately 20% of the parent is dissociated. Assuming the loss of 3 CO's for each $Fe(CO)_5$ molecule photolyzed, the CO concentration is ~60% of the initial parent concentration, which gives a rate constant for the reaction of $Fe_2(CO)_7$ with CO of 3 (±1) μs^{-1} $Torr^{-1}$ [(9 ± 3) × 10^{-11} cm^3 $molecule^{-1}$ s^{-1}]. The reported error for this rate constant is based on the error in the rate data combined with the error in the $Fe(CO)_5$ concentration and percentage of photolysis.

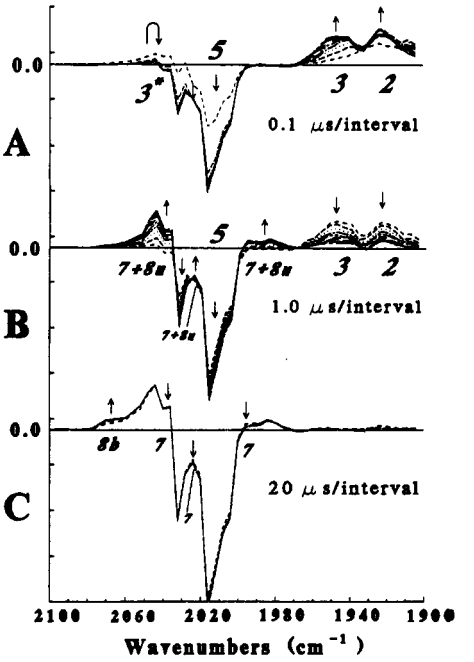

Figure 6. Time-resolved spectra generated upon 248-nm photolysis of $Fe(CO)_5$. The photolysis flow cell contained 10 mTorr of $Fe(CO)_5$ with 3 Torr of argon buffer gas. Panels A and B are segmented into 10 equal time intervals with ranges of (A) 1.0 μs and (B) 10.0 μs. Panel C is segmented into 4 equal time intervals over a range of 80 μs. As in Figure 2 the arrows indicate the direction of change in absorbance of various features during the indicated time scale, and the ordinate is in arbitrary absorbance units. See text for assignments.

The position of feature 8b is consistent with an isomer of $Fe_2(CO)_8$ observed in the rare gas matrix by Poliakoff et al. and assigned as a doubly CO bridged $Fe_2(CO)_8$ species.[31] In the matrix that species absorbs at 2058 cm^{-1}, in good agreement with the 2065-cm^{-1} absorption of feature 8b, taking into account typical matrix shifts. No attempt was made to study the reaction of doubly bridged $Fe_2(CO)_8$ with CO in detail.

In summary, for the 193-nm photolysis of $Fe(CO)_5$, two photofragments are initially produced; the major photoproduct, Fe-$(CO)_2$, reacts with $Fe(CO)_5$ to form a dinuclear species that is assigned as $Fe_2(CO)_7$. $Fe_2(CO)_7$ reacts rapidly with CO produced on photolysis of $Fe(CO)_5$ to form a product assigned as an isomer of $Fe_2(CO)_8$. On the basis of matrix data, this form of $Fe_2(CO)_8$ is likely to be a doubly bridged isomer. The assignment of the other observed initial photoproduct as Fe(CO) is based on considerations of the energetics of the photodissociation process, the behavior of the species in the presence of rare gas, and its reactive behavior. The possibility that this species is an electronically excited state of $Fe(CO)_3$, as was previously discussed,[20] is considered unlikely but cannot be completely ruled out. It is much less likely that this species is an excited electronic state of $Fe(CO)_2$. With the assignment of this minor photoproduct as Fe(CO), the species formed by the reaction of Fe(CO) and $Fe(CO)_5$ is most likely $Fe_2(CO)_6$.

B. 248-nm Photolysis of $Fe(CO)_5$. 1. Initial Photoproducts. Time-resolved IR spectra of $Fe(CO)_5$, photolyzed by 248-nm excimer radiation, are displayed in Figure 6. Figure 6A illustrates the change in the spectrum observed on a 1.0-μs time scale. Initial photolysis results in parent loss (feature 5) and appearance of two distinct coordinatively unsaturated iron carbonyl photofragment

(31) Poliakoff, M.; Turner, J. J. *J. Chem. Soc. A* **1971**, 2403.

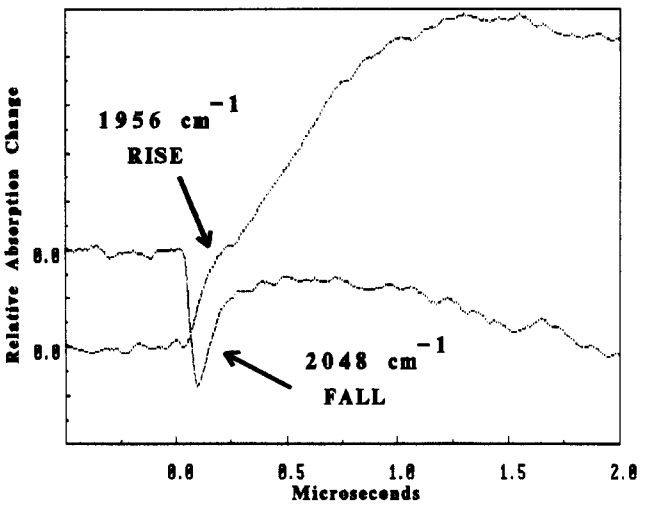

Figure 7. Single-frequency time-resolved signals generated upon 248-nm photolysis of $Fe(CO)_5$ show that the decay of the feature labeled as the 3* absorption in Figure 6 at 2048 cm^{-1} (shown inverted) matches the rise of $Fe(CO)_3$ at 1956 cm^{-1}. The part of the signal labeled "FALL" is due to the decay of 3*. The part of the signal labeled "RISE" results from formation of the ground-state $Fe(CO)_3$ species. See text for further discussion. The pressure of $Fe(CO)_5$ is 0.010 Torr.

absorptions assigned in ref 20 as $Fe(CO)_2$ (feature 2) and $Fe(CO)_3$ (feature 3). Consistent with these assignements, $Fe(CO)_3$ is observed to have significant internal excitation relative to $Fe(CO)_2$ as evidenced by the shifting and narrowing of the absorption to higher frequencies as the species is collisionally relaxed.[15,23] In contrast, $Fe(CO)_2$ centered at 1920 cm^{-1} is born with little internal excitation. This lack of vibrational excitation is best seen by ignoring the first trace in feature 2 [where vibrationally/rotationally excited $Fe(CO)_3$ overlaps feature 2] and focusing on subsequent traces where feature 3 is still shifting to higher frequencies while feature 2 grows in without observable shifting.

In the study in ref 20 an absorption was also observed in the region between 2000 and 1980 cm^{-1}, which is the region in which $Fe(CO)_4$ absorbs. As a consequence $Fe(CO)_4$ was indicated as a possible photoproduct following KrF photolysis of $Fe(CO)_5$. As can be seen from Figure 6, in this study, using a diode laser that can probe frequencies at which CO does not absorb, there is no observable absorption due to a metal carbonyl photofragment in this region. Thus, the absorption in this region observed in ref 20 was due to internally excited CO, and if $Fe(CO)_4$ is formed on KrF photolysis, it is formed in imperceptible amounts.

A curious aspect of the spectrum in Figure 6A is that the species labeled feature 3* is formed at a detector-limited rate and subsequently decays at a rate that equals the rise rate of $Fe(CO)_3$ (feature 3). This decay rate is much too rapid, at these parent pressures, to be the result of reaction of an initial photoproduct with $Fe(CO)_5$. The behavior of the feature labeled as 3* can be seen more clearly in Figure 7, where single-frequency time-resolved signals for feature 3* at 2048 cm^{-1} and for $Fe(CO)_3$ at 1956 cm^{-1} are compared. The 3* absorption at 2048 cm^{-1} is shown inverted in Figure 7 to demonstrate that the decay of the 3* absorption matches the initial rise of $Fe(CO)_3$ at 1956 cm^{-1}. The continued rise of the 1956-cm^{-1} signal after the 2048-cm^{-1} signal has completely decayed is due to the collisional relaxation of the vibrationally excited ground-state $Fe(CO)_3$. The 2048-cm^{-1} signal shows a noticeable downturn (of the inverted signal) after approximately 1.0 μs that results from the onset of dinuclear formation from the reaction of $Fe(CO)_3 + Fe(CO)_5$. As will be discussed further below, feature 3* is best assigned to an absorption of an excited state of $Fe(CO)_3$ that relaxes to the ground-state $Fe(CO)_3$ by collisions with the argon buffer gas at a rate of $\sim 5 \times 10^{-11}$ cm^3 $molecule^{-1}$ s^{-1}. This rate is $\sim 1/6$th of the gas kinetic rate of $\sim 3 \times 10^{-10}$ cm^3 $molecule^{-1}$ s^{-1} for these collision partners. This relaxation rate is sufficiently rapid that it effectively precluded the study of reactions of $Fe(CO)_3$* with parent or CO. $Fe(CO)_3$ was first observed by Poliakoff[32] in low-temperature, inert gas, matrices with IR absorptions at approximately 1930 and 2040 cm^{-1}. These frequencies are near those of features 3 and 3*, respectively, in Figure 6A (see Table I for frequencies) taking into account the fact that significant shifts to lower frequencies are often observed for matrix-isolated species when corresponding them to their gas-phase absorptions. Changes in frequency of 8 and 26 cm^{-1} are compatible with the range of typical matrix shifts. The presence of two distinct absorptions in the matrix isolation experiment was used as justification for assignment of a C_{3v} structure to $Fe(CO)_3$ (with two IR-active modes, $A_1 + E$).

Poliakoff observed that changing from a more to less interactive matrix material ($Xe \rightarrow CH_4 \rightarrow Kr \rightarrow Ar$) resulted in a decrease in intensity of the high-frequency $Fe(CO)_3$ matrix band relative to the low-frequency matrix band, while the $Fe(CO)_3$ matrix band at low frequency shifted to higher wavenumbers. Quite striking was evidence for a $Fe(CO)_3N_2$ complex forming in an N_2 matrix. These effects suggest that the $Fe(CO)_3$ species can be distorted by the interactions with even relatively inert matrix materials. Poliakoff did not rule out the possibility that interaction with the matrix resulted in distortion of $Fe(CO)_3$ from a planar D_{3h} structure that would have one IR-active mode.

Since feature 3* disappears at the same rate that 3 appears (see Figure 7), it seems clear that 3* is a precursor to the formation of 3. Correlated with the decrease in the amplitude of the high-frequency 3* band is a shift of the low-frequency band belonging to $Fe(CO)_3$. As discussed further below, this correlation implies distinct absorptions for the excited- and ground-state species. Ground-state $Fe(CO)_3$ has an absorption at 1950 cm^{-1} which correlates with the 1930-cm^{-1} absorption observed for this species in an Argon matrix.[32] No obvious higher frequency band is observed for the ground state of $Fe(CO)_3$ in the vicinity of 2040 cm^{-1}, where is would be expected on the basis of matrix data. Whether such an absorption is simply too weak to observe or completely lacking is difficult to discern because of the finite signal to noise level of the experiments and the subsequent growth of absorptions due to polynuclear species in this higher frequency region of the spectrum. A weak high-frequency band is compatible with the trend in relative band intensities observed in matrix isolation studies of $Fe(CO)_3$: more weakly interacting matrices produced smaller ratios for the absorbance of the high-frequency to low-frequency bands. By analogy the gas phase would be expected to be a very "weakly interacting environment" with a correspondingly small ratio for these absorbances. However, it is worth noting that a D_{3h} structure for the ground state of $Fe(CO)_3$ would be expected to possess only one carbonyl absorption band. Though current theoretical treatments support a C_{3v} structure for the triplet ground-state $Fe(CO)_3$ with a relatively small angle of distortion from planar,[33] it is worth noting that the experimental data in this study are not inconsistent with a planar structure for the ground state of $Fe(CO)_3$.

It is possible that the 3* absorption is due to a vibrationally excited form of $Fe(CO)_3$ which is sufficiently excited to be distorted from its equilibrium geometry, leading to enhancement of a second absorption band. However, 3* does not show significant shifting or narrowing of its absorption band which might be expected to accompany vibrational relaxation. Instead, as can be seen in Figure 6A, vibrational relaxation of the ground state of $Fe(CO)_3$ continues even after 3* has completely decayed and, therefore, is more compatible with an assignment of 3* to photogenerated, electronically excited $Fe(CO)_3$ which decays to the electronic ground state of $Fe(CO)_3$.

2. Reactions of Photoproducts following 248-nm Photolysis. The two ground-state photoproducts produced on 248-nm photolysis of $Fe(CO)_5$ react with the parent $Fe(CO)_5$ and form dinuclear products as seen in the time-resolved spectrum in Figure 6B. In Figure 6B, $Fe(CO)_2$ (feature 2) and $Fe(CO)_3$ (feature 3) decay with a corresponding parent decay while dinuclear product absorptions, labeled features 7 and 8u, grow in. The

(32) Poliakoff, M. *J. Chem. Soc., Dalton Trans.* **1974**, 210.
(33) Burdett, J. K. *Faraday Trans. 2* **1974**, *70*, 1599. Burdett, J. K. *Molecular Shapes*; John *Wiley* & Sons: New York, 1980.

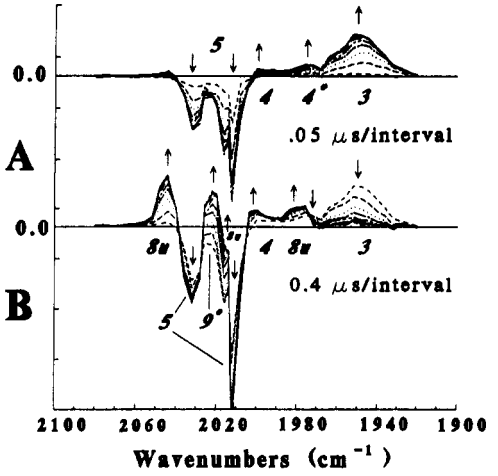

Figure 8. Time-resolved spectra generated upon 351-nm photolysis of $Fe(CO)_5$. The photolysis flow cell contained 80 mTorr of $Fe(CO)_5$ with 3 Torr of argon buffer gas. Panels A and B are segmented into 10 equal time intervals with ranges of (A) 0.5 μs and (B) 4.0 μs. As in Figure 2, the arrows indicate the direction of change in absorbance of various features during the indicated time scale, and the ordinate is in arbitrary absorbance units. See text for assignments.

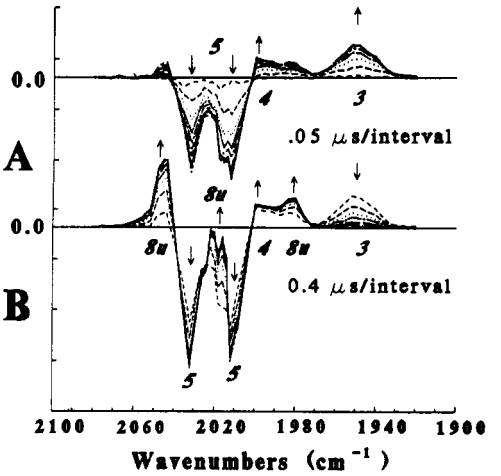

Figure 9. Time-resolved spectra generated upon 351-nm photolysis of $Fe(CO)_5$. The photolysis flow cell contained 80 mTorr of $Fe(CO)_5$ with 30 Torr of argon buffer gas. Panels A and B are segmented into 10 equal time intervals with ranges of (A) 0.5 μs and (B) 4.0 μs. As in Figure 2, the arrows indicate the direction of change in absorbance of various features during the indicated time scale, and the ordinate is in arbitrary absorbance units. See text for assignments.

product of the reaction of $Fe(CO)_2 + Fe(CO)_5$ is assigned to the same $Fe_2(CO)_7$ species (feature 7), produced following 193-nm photolysis of $Fe(CO)_5$. The $Fe_2(CO)_7$ absorption in Figure 6B matches the $Fe_2(CO)_7$ absorption in Figure 2B.

$Fe_2(CO)_7$ formed on 248-nm photolysis is observed to react with the nascent CO in the same manner as was observed following its formation on 193-nm photolysis of $Fe(CO)_5$. The spectrum in Figure 6C illustrates the changes that occur as a result of this reaction. The product of the reaction of $Fe_2(CO)_7 + CO$ (nascent) leads to an absorption labeled as feature 8b. As discussed in section III.A.2, this reaction product is assigned as a doubly bridged $Fe_2(CO)_8$ species. As expected, the long time scale decay of the $Fe_2(CO)_7$ absorption agrees well with the long time scale rise of the absorption of bridged $Fe_2(CO)_8$. The rate constant for this reaction of 3 ($\pm$1) μs^{-1} $Torr^{-1}$ [(9 $\pm$ 3) $\times$ 10^{-11} cm^3 $molecule^{-1}$ s^{-1}], which for this measurement is based on 10% of the $Fe(CO)_5$ being photolyzed and 2.5 CO molecules being produced for every $Fe(CO)_5$ molecule dissociated, is in excellent agreement with the rate constant for the $Fe_2(CO)_7 + CO$ (nascent) reaction observed following 193-nm photolysis. No attempt was made to study in detail the reaction of CO with doubly bridged $Fe_2(CO)_8$.

The product of the $Fe(CO)_3 + Fe(CO)_5$ reaction is assigned as the unbridged $Fe_2(CO)_8$ isomer on the basis of a comparison with $Fe_2(CO)_8$ observed in matrix isolation studies. This unbridged $Fe_2(CO)_8$ isomer is better isolated upon 351-nm photolysis of $Fe(CO)_5$ where the reaction of $Fe(CO)_3 + Fe(CO)_5$ can be followed without complications due to the presence of $Fe_2(CO)_7$ [which absorbs in the same region as unbridged $Fe_2(CO)_8$]. Therefore, the kinetics of formation of unbridged $Fe_2(CO)_8$ and further discussions regarding its assignment are presented in section III.C.2 dealing with 351-nm photolysis of $Fe(CO)_5$.

A relatively small change observed in the spectra in Figure 6, which cannot be explained by the reaction of either $Fe(CO)_2$ or $Fe(CO)_3$ with $Fe(CO)_5$ or the reaction of the dinuclear species with nascent CO, is best assigned to a rapid reaction of a dinuclear species with parent, forming $Fe_3(CO)_{12}$. As similar behavior is seen following 351-nm photolysis of $Fe(CO)_5$, formation of this trinuclear species will also be discussed in greater detail in section III.C.2.

To summarize the photolysis of $Fe(CO)_5$ by 248-nm radiation, three photofragments are initially produced: $Fe(CO)_2$ and $Fe(CO)_3$ and a species assigned as $Fe(CO)_3$*, which is most likely electronically excited $Fe(CO)_3$. Reactions of $Fe(CO)_5$ with $Fe(CO)_2$ to form $Fe_2(CO)_7$ and $Fe(CO)_3$ with $Fe(CO)_5$ to form unbridged $Fe_2(CO)_8$ are observed to take place at the same near gas kinetic rates as observed for the corresponding reactions occurring following 193- and 351-nm photolysis of $Fe(CO)_5$, respectively. Furthermore, a rapid reaction of $Fe_2(CO)_7$ with the CO formed as a result of photolysis takes place with a rate constant that is in good agreement with the rate constant determined for the corresponding process occurring following 193-nm photolysis. $Fe(CO)_3$* is rapidly collisionally relaxed to $Fe(CO)_3$ which has only one obvious IR band in the CO stretch region. A small amount of $Fe_3(CO)_{12}$ is formed.

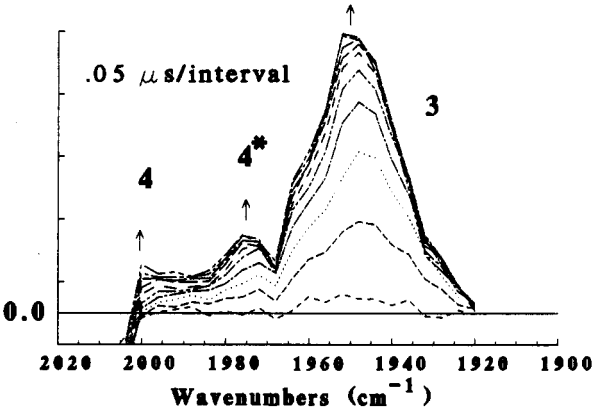

Figure 10. Time-resolved spectra generated upon 351-nm photolysis of $Fe(CO)_5$. The spectroscopic data are identical with those shown in Figure 8, but the range of wavenumbers on the abscissa is a subset of the range used in Figure 8. See text for assignments.

C. 351-nm Photolysis $Fe(CO)_5$. 1. Initial Photoproducts. Time-resolved spectra obtained on 351-nm photolysis of $Fe(CO)_5$ are displayed in Figures 8 and 9. Figure 8 depicts a spectrum obtained at a low buffer gas pressure (3 Torr of argon) while Figure 9 displays the same spectrum at a higher buffer gas pressure (30 Torr of argon). It will be shown that the difference between these spectra results from reaction of one of the initial photoproducts, which is assigned as an electronically excited state of $Fe(CO)_4$ that can be collisionally relaxed to ground-state $Fe(CO)_4$.

The 50 ns/interval spectra in Figure 8A and 9A clearly demonstrate the effect of a buffer gas pressure change on the initial photofragment absorptions. The initial photoproduct, which leads to feature 3, has been assigned to the same $Fe(CO)_3$ species as was observed upon 248-nm photolysis.[20] Feature 4 was assigned to $Fe(CO)_4$ on the basis of a direct reaction with CO to form parent.[20] Also, as expected for a more saturated (lower energy) species, feature 4 is formed with significant vibrational excitation (as can be seen in the collisional relaxation of feature 4 in the spectrum in Figure 9A) while feature 3 is born with little if any

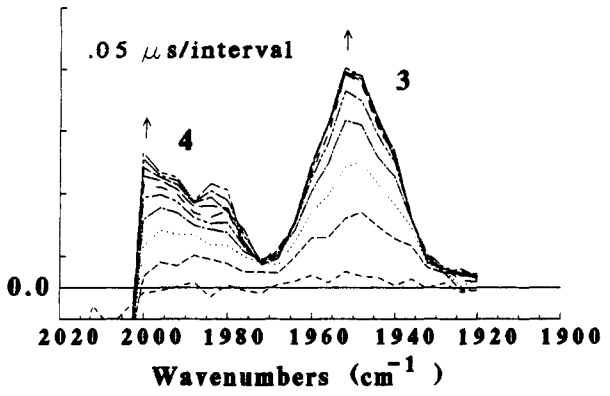

Figure 11. Time-resolved spectra generated upon 351-nm photolysis of $Fe(CO)_5$. The spectroscopic data are identical with those shown in Figure 9, but the range of wavenumbers on the abscissa is a subset of the range used in Figure 9. See text for assignments.

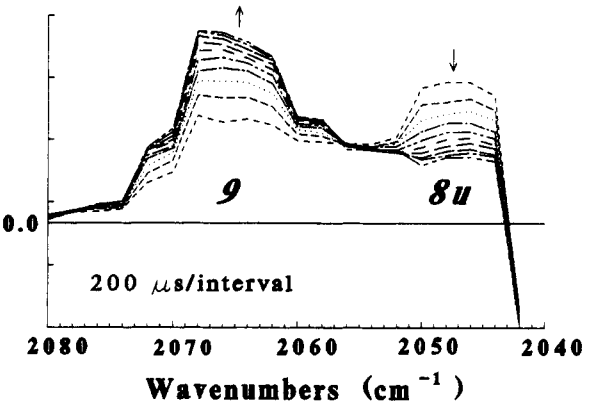

Figure 12. Time-resolved spectrum generated upon 351-nm photolysis of $Fe(CO)_5$. The photolysis flow cell contained 0.5 Torr of $Fe(CO)_5$ with 5 Torr of CO and 12.5 Torr of argon buffer gas. The data are shown in 10 equal intervals over a range of 2.0 ms. The reaction of unbridged $Fe_2(CO)_8 + CO \rightarrow Fe_2(CO)_9$ leads to decay of feature 8u, assigned to unbridged $Fe_2(CO)_8$ in the text, and the rise of feature 9, assigned to ground-state $Fe_2(CO)_9$. Arrows indicate the direction of change of the absorption features.

vibrational excitation. A comparison between the partial time-resolved spectra at 50 ns/interval and 3 Torr of argon in Figure 10 and at 30 Torr of argon in Figure 11 indicates there is an absorption centered at 1975 cm^{-1} (feature 4* in Figure 8 and Figure 10) that *only forms at the low buffer gas pressure.* This absorption is at a lower frequency than either of the two $Fe(CO)_4$ absorptions.

Since the species that corresponds to feature 4* is relaxed on collisions with rare gas, its behavior is similar to that observed for the species assigned in section III.B.1 as $Fe(CO)_3$*, an excited electronic state of $Fe(CO)_3$. On the basis of energy considerations, an assignment to the lowest excited singlet state of $Fe(CO)_4$ appears more reasonable than an assignment to an excited state of a more highly unsaturated excited-state species such as singlet $Fe(CO)_3$.

The best estimate for the CO bond dissociation energy for the $Fe(CO)_3$–(CO) species is on the order of 0.5 eV, which would put the ground state of $Fe(CO)_3$ ~2.3 eV above the ground state of $Fe(CO)_5$.[26] The first excited singlet state of $Fe(CO)_3$ was calculated by Guenzburger et al. to be 1.2 eV above the ground-state $Fe(CO)_3$.[24] Thus the energy of the first excited state of $Fe(CO)_3$ would be ~3.5 eV above the $Fe(CO)_5$ ground state. Although this energy is comparable to the 3.53 eV energy of a 351-nm photon, there is very little if any energy left over for CO excitation. Hepburn and co-workers[17] found that the CO energies following 351-nm photolysis could be fit to a statistical CO distribution compatible with ~0.4 eV of internal excitation per CO that is lost. On the basis of this data we believe it is unlikely that feature 4* in Figure 10 is due to an excited state of $Fe(CO)_3$.

Formation of the first excited electronic state of $Fe(CO)_4$, on the other hand, is energetically very feasible. The ground state of $Fe(CO)_4$ was measured to be ~1.8 eV above the $Fe(CO)_5$ ground state by Lewis et al.[34] The first excited singlet state of $Fe(CO)_4$ was calculated by Guenzburger et al. to be approximately 0.2 eV above the ground state,[24] while Veillard calculated an energy for the excited $Fe(CO)_4$ species that is about 1.1 eV above the $Fe(CO)_4$ ground state.[35] Even with the higher value, production of a singlet $Fe(CO)_4$ species would require 2.9 eV of the 3.53 eV of energy available from a 351-nm photon, leaving in excess of ~0.6 eV to be disposed among the internal states of CO and the $Fe(CO)_4$ photofragments.

Finally, as discussed in the following section, the reaction kinetics of the species labeled 4* significantly aids in assigning the species to an excited singlet state of $Fe(CO)_4$.

2. Reactions of Photoproducts following 351-nm Photolysis. The time-resolved spectrum in Figure 9B illustrates the decay of $Fe(CO)_3$ (feature 3) on reaction with parent (feature 5) to form the unbridged isomer of $Fe_2(CO)_8$ (feature 8u) which was also observed as a product of the same reaction following 248-nm photolysis of $Fe(CO)_5$. The assignment of feature 8u to an unbridged $Fe_2(CO)_8$ species is based principally on a comparison with the matrix isolation study of $Fe_2(CO)_9$ photolysis by Poliakoff et al.[31,36] The gas-phase absorptions in Figures 8B and 9B for feature 8u, at 2046, 2016, and 1982 cm^{-1}, match well with the absorptions of matrix isolated unbridged $Fe_2(CO)_8$ at 2042 and 2009 cm^{-1} (both strong) and at 1987 and 1979 cm^{-1} (both weak).[31] Since gas-phase absorptions typically have widths on the order of tens of wavenumbers, the two low-frequency bands would not be expected to be resolved in the gas phase due to the relatively small difference in the peak frequencies observed in the matrix.

The dependence of the decay rate of $Fe(CO)_3$ and the rise rate of the unbridged $Fe_2(CO)_8$ isomer on parent pressure agree within experimental error, and each set of data gives a rate constant for this reaction of 9.5 (±1.3) μs^{-1} $Torr^{-1}$ [$(2.9 \pm 0.4) \times 10^{-10}$ cm^3 $molecule^{-1}$ s^{-1}].

Since ground-state $Fe(CO)_4$ reacts much more slowly with parent or CO than $Fe(CO)_3$, these reactions of $Fe(CO)_4$ can be studied without interferences from $Fe(CO)_3$ or $Fe(CO)_3$ reaction products since they occur on different time scales. To facilitate the study of $Fe(CO)_4$ reactions, it proved convenient to add CO to the reaction gases to build up the $Fe(CO)_4$ concentration through the rapid reaction of $Fe(CO)_3 + CO$.[20] $Fe(CO)_4$ reacts with parent to form $Fe_2(CO)_9$ (assignment discussed below) with an absorption centered at 2066 cm^{-1}. As expected, the parent pressure dependence of the rate of reaction of $Fe(CO)_4$ and formation of $Fe_2(CO)_9$ agree within experimental error and give a rate constant for reaction of $Fe(CO)_4 + Fe(CO)_5$ of $(1.7 \pm 0.5) \times 10^{-2}$ μs^{-1} $Torr^{-1}$ [$(5.2 \pm 1.5) \times 10^{-13}$ cm^3 $molecule^{-1}$ s^{-1}].

The rate of reaction of $Fe(CO)_4 + Fe(CO)_5$ is more than 2 orders of magnitude slower than observed for the reaction of $Fe(CO)_3 + Fe(CO)_5$. $Fe(CO)_4$ is known to have a triplet ground state,[14] while $Fe_2(CO)_9$ has a singlet ground state.[37] Thus this relatively slow reaction is formally spin disallowed as was observed for the slow reaction of $Fe(CO)_4 + CO$.[20] Since, as discussed below, the reaction of unbridged $Fe_2(CO)_8$ with CO is significantly slower than a gas kinetic process, it could be activated. However, a measurement of the temperature dependence of the $Fe_2(CO)_8 + CO$ reaction showed no change in reaction rate over the temperature range from 295 to 392 K [the temperature at which significant decomposition of $Fe(CO)_5$ starts to occur in our apparatus], demonstrating this is an unactivated process.

Figure 12 shows a time-resolved spectrum illustrating the changes that occur due to the reaction of $Fe_2(CO)_8$ (feature 8u)

(34) Lewis, K. E.; Golden, D. M.; Smith, G. P. *J. Am. Chem. Soc.* **1984**, *106*, 3905.
(35) Daniel, C.; Bénard, M.; Dedieu, A.; Wiest, R.; Veillard, A. *J. Phys. Chem.* **1984**, *88*, 4805.
(36) Fletcher, S. C.; Poliakoff, M.; Turner, J. J. *Inorg. Chem.* **1986**, *25*, 3597.
(37) Freundlich, H.; Cuy, E. J. *Ber.* **1923**, *56*, 2264.

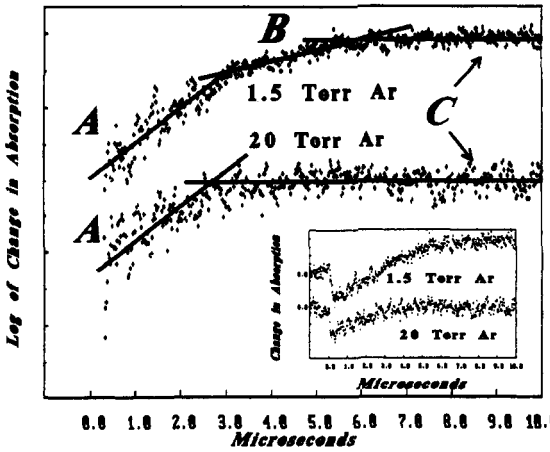

Figure 13. Single-frequency time-resolved signals taken at 2022 cm^{-1} with buffer gas pressures of 1.5 and 20 Torr. The logarithmic scale on the y-axis permits different exponential components to be distinguished. The inset shows the 2022-cm^{-1} signals with a linear y-axis scale. (Note that the inset shows an initial depletion in the first microsecond that is due to parent photolysis.) The part of the signal labeled as A corresponds to the change resulting from the formation rate of unbridged $Fe_2(CO)_8$ from the reaction of ground-state $Fe(CO)_3 + Fe(CO)_5$. The part labeled B corresponds to the product assigned to singly bridged $Fe_2(CO)_9$. C indicates the base line for the signals.

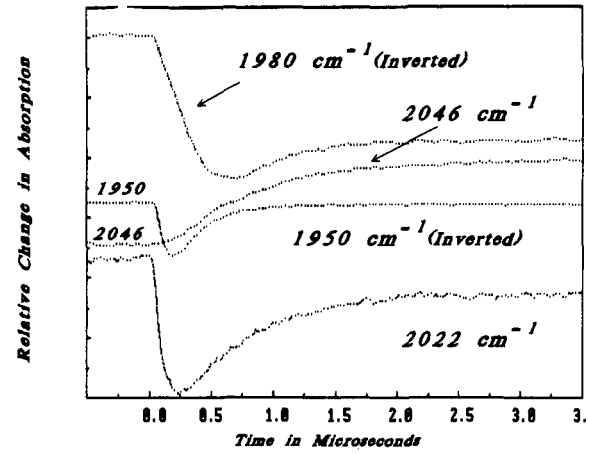

Figure 14. A plot of four single-frequency time-resolved signals generated from $Fe(CO)_5$ photolysis at 351 nm. The 1950- and 1980-cm^{-1} signals are shown inverted. See text for assignment.

with CO to form $Fe_2(CO)_9$ (feature 9). Feature 9 is assigned to the ground-state $Fe_2(CO)_9$ species on the basis of comparison to absorptions in a rare gas matrix of this stable but very involatile species.[31,32,36] Strong matrix absorptions for $Fe_2(CO)_9$[31] at 2066, 2060, 2038, and 2032 cm^{-1} correspond well to the gas-phase absorptions assigned to $Fe_2(CO)_9$ which are centered at approximately 2066, 2060 (shoulder), 2045, and 2036 cm^{-1} and also match the absorptions of the $Fe(CO)_4 + Fe(CO)_5$ reaction product. The isobestic point in Figure 12, at 2056 cm^{-1}, demonstrates that the reaction of the unbridged form of $Fe_2(CO)_8$ with CO is a simple A → B process. Again, the CO pressure dependence of the decay of the absorption due to unbridged $Fe_2(CO)_8$ and the rise of the absorption due to $Fe_2(CO)_9$ agree within experimental error to give a rate constant for this reaction of 2.5 (±0.7) × 10^{-4} μs^{-1} $Torr^{-1}$ [(7.8 ± 2.3) × 10^{-15} cm^3 $molecule^{-1}$ s^{-1}].

The minor photoproduct, assigned as $Fe(CO)_4$ in an excited singlet state (feature 4* in Figure 10) reacts with parent to form a dinuclear product as seen in Figure 8B (feature 9*). Comparison of a spectrum taken at low buffer gas pressure (Figure 8B) to a spectrum obtained at high buffer gas pressure (Figure 9B) demonstrates a marked effect on the dinuclear product absorption profile, with the most obivous change being the rise above the base line of the dinuclear species absorbing at 2022 cm^{-1}. The effect of buffer gas pressure on feature 9* at 2022 cm^{-1} is also shown in Figure 13.

Figure 13 displays the logarithm of signals obtained at 2022 cm^{-1} at buffer gas pressures of 1.5 and 20 Torr. The actual 2022-cm^{-1} signals are also shown in the inset in Figure 13. The log of the signals in Figure 13 are fit to least-square lines. (Note that the signals in the inset show an initial depletion in the first microsecond that is due to parent photolysis.) These signals demonstrate that the 9* product has a rate of formation that is slower than the rate of formation of unbridged $Fe_2(CO)_8$ from the reaction of ground-state $Fe(CO)_3 + Fe(CO)_5$. The same fast rise is observed for the two buffer gas pressures and is due to formation of unbridged $Fe_2(CO)_8$. A slower rise, observed only at the low argon pressure, is assigned to the product of the reaction of electronically excited, singlet $Fe(CO)_4 + Fe(CO)_5$. There is also a corresponding change in the decay of $Fe(CO)_5$ (probing at 2032 cm^{-1}) such that at the low buffer gas pressure both the faster and slower processes are observed in the $Fe(CO)_5$ decay while only the faster process is observed at the higher buffer gas pressure. This product corresponding to the 9* absorption in Figure 8 is most likely a transient form of $Fe_2(CO)_9$ as discussed below. An absorption for this form of $Fe_2(CO)_9$ is observed near 2050 cm^{-1}. However, that absorption is partially obscured by unbridged $Fe_2(CO)_8$ so that a precise peak position cannot be obtained.

The dinuclear product formed from the reaction of the excited singlet state of $Fe(CO)_4$ and $Fe(CO)_5$ is not consistent with the lowest energy form of $Fe_2(CO)_9$ since the most prominent absorption of the stable $Fe_2(CO)_9$ species, at 2066 cm^{-1}, does not appear in the TRIS spectrum on the time scale of formation of this species. A transient form of $Fe_2(CO)_9$, resulting from the recombination of an unobserved $Fe_2(CO)_8$ species with CO in the low-temperature rare gas matrix photolysis of $Fe_2(CO)_9$, was reported by Fletcher et al. and assigned to a singly bridged $Fe_2(CO)_9$ species.[36] This transient $Fe_2(CO)_9$ matrix species absorbs at 2049 and 2016 cm^{-1}, which is consistent with absorptions of the pressure-dependent dinuclear species observed in this gas-phase study. Fletcher et al. also refers to a similar transient absorption observed by Church in a hydrocarbon solution at room temperature. Both groups observed the subsequent decay of this transient $Fe_2(CO)_9$ species to the stable form of $Fe_2(CO)_9$. Although the singly bridged $Fe_2(CO)_9$ species is a transient in the matrix and solution, it is not surprising that the species would survive on the millisecond time scale of the gas-phase photolysis experiment. As discussed in section III.D, the assignment of Feature 9* in Figure 8B to $Fe_2(CO)_9$ in a singlet state is consistent with the rapid reaction rate observed, since the reaction of a singlet $Fe(CO)_4$ with $Fe(CO)_5$ would be spin allowed.

Addition of CO to the system can be used to further demonstrate that the excited-state $Fe(CO)_4$ species absorbing between 1984 and 1970 cm^{-1} (feature 4* in Figure 10) is indeed involved in the formation of $Fe_2(CO)_9$*. Loss of the species absorbing in this frequency region can be observed on photolysis following addition of CO to the system since the $Fe_2(CO)_8$ dinuclear product, also absorbing in this frequency region, will decrease in amplitude due to the competition set up between CO and parent in their reaction with $Fe(CO)_3$.

	relative rate
$Fe(CO)_3 + Fe(CO)_5 \rightarrow Fe_2(CO)_8$	10
$Fe(CO)_3 + CO \rightarrow Fe(CO)_4$	1

Figure 14 shows that the decay of the $Fe(CO)_4$* species at 1980 cm^{-1} can be fit to the rise of the $Fe_2(CO)_9$* absorption at 2022 cm^{-1} as well as at 2046 cm^{-1}. The decay of the $Fe(CO)_3$ absorption at 1950 cm^{-1} is also shown in Figure 14 to demonstrate that $Fe(CO)_3$ is not responsible for the product observed to grow in at 2022 and 2046 cm^{-1} after about 0.75 μs.

The rate constant for the reaction of $Fe(CO)_4$* with $Fe(CO)_5$ was measured to be 6 ± 1 μs^{-1} $Torr^{-1}$ [(1.8 ± 0.3) × 10^{-10} cm^3 $molecule^{-1}$ s^{-1})] as compared with 9.5 ± 1.3 μs^{-1} $Torr^{-1}$ for $Fe(CO)_3 + Fe(CO)_5$. A rate constant of 0.5 (±0.1) μs^{-1} $Torr^{-1}$ [(1.5 ± 0.3) × 10^{-11} cm^3 $molecule^{-1}$ s^{-1}] was measured for the depletion

of $Fe(CO)_4$* by CO. As discussed below, this rate constant is a sum of reaction and quenching rate constants and is slightly slower than the rate constant of 0.72 (±0.1) μs^{-1} $Torr^{-1}$ observed for the $Fe(CO)_3$ + CO reaction. It is clear that quenching of $Fe(CO)_4$* by CO to the ground-state $Fe(CO)_4$ species occurs. This was demonstrated by comparing the rate of $Fe(CO)_4$* decay to the rate of $Fe(CO)_4$ formation under varying pressures of Ar and CO. However, it is difficult to quantify the relative percentage of reaction of $Fe(CO)_4$* with CO versus quenching of $Fe(CO)_4$* by CO. The growth of the expected $Fe(CO)_5$ reaction product is obscured by the growth of $Fe_2(CO)_8$ and $Fe_2(CO)_9$*, both of which deplete parent and both of which absorb in the same spectral region as parent. It also has not been possible to probe in detail whether reactions of $Fe(CO)_4$* are taking place in "high-pressure limit" under experimental conditions since, as was discussed, $Fe(CO)_4$* is efficiently collisionally quenched to $Fe(CO)_4$.

As described previously, the singlet excited states of both $Fe(CO)_3$ and $Fe(CO)_4$ are efficiently collisionally relaxed to their respective ground states. The cross sections for collisional relaxation of singlet $Fe(CO)_3$ and singlet $Fe(CO)_4$ are approximately 1/6 and 1/40 gas kinetic, respectively, for collisions with Ar. The only other electronically excited metal carbonyl species for which we are aware of lifetime data is coordinatively unsaturated $Ni(CO)_3$, which is formed on 308-nm photolysis of $Ni(CO)_4$. Electronically excited $Ni(CO)_3$ has a radiative lifetime of 12 μs as measured in the collision-free environment of a molecular beam.[38] No data are available on the number of collisions required to relax as excited electronic state of a metal carbonyl species, but collisions have been observed to enhance singlet–triplet crossing in organic systems.[39]

Finally, another minor product is observed to form following both 351- and 248-nm photolysis. On the basis of a strong absorption at 2066 cm^{-1} and other characteristic absorptions in the 1800–1900-cm^{-1} region, we believe this species is $Fe_3(CO)_{12}$. As expected, the rise time of this species is slower than the rise times of $Fe_2(CO)_8$ isomers which are presumably its precursor. Consistent with this interpretation, a decay of parent $Fe(CO)_5$ is observed, which agrees with the rise time of $Fe_3(CO)_{12}$, implying that the rate-limiting step in formation of $Fe_3(CO)_{12}$ is reaction of a coordinatively unsaturated species with $Fe(CO)_5$. However, we have not been able to find a polynuclear species that decays on this time scale. The most likely reason for this is either the amount of $Fe_3(CO)_{12}$ is so small that we cannot easily detect this decay in the presence of other processes and/or that $Fe_3(CO)_{12}$ forms from a species whose absorptions significantly overlap the absorptions of other species in the system. We favor this latter possibility. Providing some support for this latter interpretation is the observation by Fletcher et al. of a very rapid CO addition reaction of a species formed on photolysis of $Fe_2(CO)_9$ to produce a singly bridged isomer of $Fe_2(CO)_9$.[36] It was speculated that this photoproduct was a third isomer of $Fe_2(CO)_8$. Since Fletcher et al. did not directly observe this form of $Fe_2(CO)_8$ because of its very rapid reaction with CO and we do not observe it, there is no information regarding its IR absorption spectrum. However, the formation of $Fe_3(CO)_{12}$ from the reaction of the unobserved dinuclear species with $Fe(CO)_5$ was measured, as a function of $Fe(CO)_5$ pressure, and found to have a rate constant of 3 ± 1 μs^{-1} $Torr^{-1}$ [(9.0 ± 3.0) × 10^{-11} cm^3 $molecule^{-1}$ s^{-1}]. Addition of 1 Torr of CO completely suppressed growth of $Fe_3(CO)_{12}$, demonstrating that CO also reacts rapidly either with the dinuclear precursor and/or with the coordinatively unsaturated species that leads to the dinuclear precursor.

Interestingly, all other reactions that have been considered which lead to the formation of polynuclear metal species have retained, in the final product, all the CO's that were present in the reactants. This does not appear to be the case for the reaction which forms $Fe_3(CO)_{12}$ if the dinuclear precursor is, as expected, $Fe_2(CO)_8$. Yet, this latter reaction has precedence, although under quite different conditions. Suslick et al. postulate $Fe_3(CO)_{12}$ formation by high-intensity ultrasound by the same pathway: formation of $Fe_2(CO)_8$ from $Fe(CO)_3$ + $Fe(CO)_5$ followed by further reaction with $Fe(CO)_5$.[40] Jackson and Trusheim observe exclusively $Fe_3(CO)_{12}$ after photolysis of $Fe(CO)_5$ adsorbed on silica, and they postulate a mechanism that involves an $Fe_2(CO)_8$ precursor.[6] Others have also reported photochemical formation of $Fe_3(CO)_{12}$ on silica.[7] $Fe_3(CO)_{12}$ has also been reported as a product of photolysis of $Fe(CO)_4L$ complexes in solution.[41,42] A potential difference between this reaction and all the others we have reported on is that, with retention of CO ligands, the other reactions lead to either coordinatively unsaturated species or stable saturated species. Retention of CO's following the reaction of $Fe_2(CO)_8$ with $Fe(CO)_5$ would lead to a species that has *more than* the required number of electrons to satisfy the 18-electron rule.

It is also interesting that the dinuclear iron carbonyls appear to have multiple isomers on the millisecond time scale of the TRIS experiment. Poliakoff has reported at least three $Fe_2(CO)_8$ isomers and two $Fe_2(CO)_9$ isomers in inert gas matrices.[36,43] It appears that polynuclear species with CO bridges can form rapidly. The formation of the species assigned to doubly bridged $Fe_2(CO)_8$ takes place on a gas-kinetic time scale through the reaction of $Fe_2(CO)_7$ + CO. Either CO bridges form in the $Fe_2(CO)_7$ + CO reaction (either promptly or during vibrational relaxation of the product) or $Fe_2(CO)_7$ already possesses bridging CO ligands formed in the rapid reaction of $Fe(CO)_2$ + $Fe(CO)_5$. Some evidence supporting the latter possibility comes from a study of a compound, $(C_4R_4)_2Fe_2(CO)_3$, which is isoelectronic with $Fe_2(CO)_7$. A crystal structure of this compound shows that it contains three bridging CO ligands.[44] If $Fe_2(CO)_7$ also contains three bridging CO's, reaction of $Fe_2(CO)_7$ with CO to produce the observed doubly bridged $Fe_2(CO)_8$ would likely result in the migration of a bridging CO with it becoming a CO donating two electrons to a single metal atom.

Finally, a remarkable feature in the formation of some of the polynuclear metal carbonyls in this and other studies[29,44,45] is the magnitude of the rate constant which can approach gas kinetic. Such large rate constants seem incompatible with the steric requirements involved in the direct collisional formation of many of the polynuclear metal carbonyls. This suggests that an internally excited complex is the initial product in such a reaction with internal excitation facilitating rearrangement which in conjunction with energy relaxation processes ultimately leads to the observed geometry of the polynuclear species. Direct observation of such dynamical processes is masked by internal excitation which broadens the infrared bands of these species.

In summary, 351-nm photolysis of $Fe(CO)_5$ results in two major photoproducts: $Fe(CO)_3$ and $Fe(CO)_4$ in their ground states. Following the expected trend, $Fe(CO)_4$ is born with significant vibrational excitation while nascent $Fe(CO)_3$ is produced with negligible vibrational excitation. At low buffer gas pressures another transient species is observed that is most likely an excited singlet state of $Fe(CO)_4$. This species is efficiently collisionally quenched, and in contrast to the triplet ground state of $Fe(CO)_4$, it reacts rapidly with $Fe(CO)_5$ to form $Fe_2(CO)_9$. The absorptions of the $Fe_2(CO)_9$ product correspond best to those reported in matrix isolation studies for a transient singly bridged structure which, in the matrix, subsequently decayed to the ground state, triply bridged $Fe_2(CO)_9$ species. However, no decay of this $Fe_2(CO)_9$ species could be observed on a millisecond time scale under our reaction conditions. The reaction of ground-state $Fe(CO)_3$ with $Fe(CO)_5$ produces an unbridged isomer of $Fe_2(CO)_8$. Unbridged $Fe_2(CO)_8$ subsequently reacts with CO to form

(38) Rösch, N.; Jörg, H.; Kotzian, M. *J. Chem. Phys.* **1987**, *86*, 4038.
(39) Kommandeur, J.; Majewski, W. A.; Meerts, W. L.; Pratt, D. W. *Annu. Rev. Phys. Chem.* **1987**, *38*, 433 and references therein.
(40) Suslick, K. S.; Schubert, P. F.; Goodale, J. W. *J. Am. Chem. Soc.* **1981**, *103*, 7342.
(41) Koerner von Gustorf, E. A.; Henry, M. C.; Di Pietro, C. *Z. Naturforsch.* **1966**, *21B*, 42.
(42) Schubert, E. H.; Sheline, R. K. *Inorg. Chem.* **1966**, *5*, 1071.
(43) Poliakoff, M.; Turner, J. J. *J. Chem. Soc. A* **1971**, 654.
(44) Murahashi, S.-I.; Mizoguchi, T.; Hosokawa, T.; Moritani, I. *J. Chem. Soc., Chem. Commun.* **1974**, 563.
(45) Bogdan, P. L.; Weitz, E. *J. Am. Chem. Soc.* **1990**, *112*, 639.

TABLE I

species	gas-phase frequencies, cm^{-1}	matrix frequencies,[a] cm^{-1}	reaction rates, cm^3 molecule^{-1} s^{-1} +$Fe(CO)_5$	reaction rates, cm^3 molecule^{-1} s^{-1} +CO	spin conserving
$Fe(CO)$	1945		$(8.6 \pm 2.5) \times 10^{-11}$		yes
$Fe(CO)_2$	1920		$(3.7 \pm 0.6) \times 10^{-10}$	$(3.0 \pm 0.5) \times 10^{-11}$ [b]	yes
$Fe(CO)_3$	1950	1930 2040	$(2.9 \pm 0.4) \times 10^{-10}$	$(2.2 \pm 0.33) \times 10^{-11}$ [b]	yes
$Fe(CO)_3$*	2045				
$Fe(CO)_4$[c]	2000 1984	1992 1967	$(5.2 \pm 1.5) \times 10^{-13}$	$(5.2 \pm 1.2) \times 10^{-14}$ [b]	no
$Fe(CO)_4$*	1975		$(1.8 \pm 0.3) \times 10^{-10}$		yes
$Fe_2(CO)_6$	2055				
$Fe_2(CO)_7$	2045 2025 2000 1950		[d]	$(9 \pm 3) \times 10^{-11}$	yes
$Fe_2(CO)_8$ (unbridged)	2046 2016 1982	2042 2009 1987 vw, 1979 w, br	[d]	$(7.8 \pm 2.3) \times 10^{-15}$	no
$Fe_2(CO)_8$ (bridged)	2065	2058 vs 2034 s 2024 s 1867 w, 1826 w	[d]	[d]	
$Fe_2(CO)_9$	2066 2060 2045 2036	2066 vs 2060 sh 2038 vs 2032 s			
$Fe_2(CO)_9$*	2050 2022	2049 2016			
$Fe_3(CO)_{12}$	2080–2045 2025 1870's 1830's	2058 2053 2036 2013 1870 1833	$(9 \pm 3.0) \times 10^{-11}$ [e]		yes

[a] References 31, 32, 36, and 43. [b] Reference 20. [c] Rates of reactions of $Fe(CO)_4$ with H_2 and O_2 have also been measured. [d] Not studied. [e] Rate of formation of $Fe_3(CO)_{12}$ from $Fe(CO)_5$ + dinuclear iron carbonyl (see text for discussion).

ground-state $Fe_2(CO)_9$ in a slow reaction. Ground-state $Fe(CO)_4$ reacts slowly with $Fe(CO)_5$ to form ground-state $Fe_2(CO)_9$ in a slow reaction. $Fe_3(CO)_{12}$ is observed to form rapidly, most likely by reaction of a minor $Fe_2(CO)_8$ dinuclear species with $Fe(CO)_5$.

D. Reactions of Coordinatively Unsaturated Iron Carbonyls and Spin Selection Rules. Table I summarizes the rate constants determined in this study for reactions of coordinatively unsaturated iron carbonyl species with both CO and parent. Also listed are previously determined rate constants for reactions of these species with CO, principally from ref 20. Inspection of this table reveals that many of the rate constants are near gas kinetic. Specifically, reactions of $Fe(CO)_2$, $Fe(CO)_3$, and the excited electronic state of $Fe(CO)_4$ with parent are all within approximately a factor of 3 of gas kinetic. The rate constant for the reaction of $Fe(CO)$ with parent is not much smaller. Rate constants of similar magnitude have been observed for reactions of coordinatively unsaturated metal carbonyls with parent in a variety of other systems including the $Cr(CO)_x$, $Os(CO)_x$, and $Ru(CO)_x$ species.[29,45,46] However, it is interesting to note that the reaction of the ground state of $Fe(CO)_4$ with parent is approximately 3 orders of magnitude smaller than the rate constants for the processes mentioned above. Similar disparities in the magnitude of the rate constants for CO addition reactions also exist. Note that the addition of CO to $Fe(CO)_2$, $Fe(CO)_3$, and $Fe_2(CO)_7$ are all within approximately an order of magnitude of gas kinetic while addition of CO to the ground state of $Fe(CO)_4$ and to the unbridged isomer of $Fe_2(CO)_8$ is between 4 and 5 orders of magnitude less than gas kinetic.

In ref 20 the differences in rate constants for CO addition to mononuclear iron carbonyls was explained on the basis of spin conservation in this addition reaction. It is known that $Fe(CO)_4$ has a ground state that is a triplet[14] while the ground state of $Fe(CO)_5$ is a singlet. Thus the addition of CO, with a singlet ground state, to $Fe(CO)_4$ to form $Fe(CO)_5$ is formally spin disallowed, and this reaction has been observed to be much slower than CO addition to the other mononuclear iron carbonyls or in fact to virtually any other coordinatively unsaturated mononuclear metal carbonyl that has been studied.[15,45,46] This includes CO addition reactions of the tetracarbonyls of the other group VIII metals, which are near gas kinetic, indicating that there is not something unusual about addition of CO to a C_{2v} tetracarbonyl that leads to a slow reaction. These other group VIII tetracarbonyls have been calculated to have singlet ground states.[45,46] Thus, spin conservation seems to be a significant factor in determining the rate of CO addition reactions. Then, by implication the CO addition reactions of $Fe(CO)_2$ and $Fe(CO)_3$ should be spin allowed. Since $Fe(CO)_4$ has a triplet ground state, this implies that both $Fe(CO)_3$ and $Fe(CO)_2$ also have triplet ground states. This conclusion has been discussed in more detail in ref 15.

The differences in the rate constants in Table I are compatible with spin conservation playing an important role in determining the magnitude of rate constants in these reactions. An example of this involves the excited state of $Fe(CO)_4$ that is produced on 351-nm photolysis of $Fe(CO)_5$. This species is assigned as the first excited singlet state of $Fe(CO)_4$. Rapid reaction of $Fe(CO)_4$* with parent to form an isomer of $Fe_2(CO)_9$ that has been previously observed in a matrix is in contrast with the relatively slow reaction of the ground state of $Fe(CO)_4$ with $Fe(CO)_5$. As discussed in more detail below, this behavior is compatible with a singlet ground state for this isomer of $Fe_2(CO)_9$. Thus the rapid reaction to form this species is spin allowed.

Further evidence of the influence of spin on the rate of reactions in these systems comes from studies of the reaction of the ground state of $Fe(CO)_4$ with some diatomic molecules other than CO. O_2 has a $(X^3\Sigma_g^-)$ ground state, thus a reaction of this triplet species with triplet ground state $Fe(CO)_4$ might be expected to lead to a larger rate constant for reaction than with a single reactant. Triplet organic diradicals, for example, are observed to react rapidly with ground-state O_2 while analogous singlet diradicals show greatly reduced reactivity.[47] Indeed, a rate constant of 0.10

(46) Bogdan, P. L.; Weitz, E. *J. Am. Chem. Soc.* **1990**, *111*, 3163.

(± 0.03) μs^{-1} $Torr^{-1}$ (3.1×10^{-12} cm^3 $molecule^{-1}$ s^{-1}) has been measured for the reaction of $Fe(CO)_4 + O_2$, which is more than 50 times larger than the spin-disallowed addition reaction of CO to $Fe(CO)_4$. This rate constant is the same order of magnitude (though somewhat smaller) as the rate constants for the "spin-allowed" addition of CO to $Fe(CO)_2$ and $Fe(CO)_3$. For these measurements, the O_2 pressure was varied over the range of 1–6 Torr by using an argon buffer gas to bring the total pressure to 10 Torr. The $Fe(CO)_5$ pressure was 0.05 Torr. These measurements were meant only to examine relative rates by using conditions similar to those under which spectra were obtained. As such, it is possible that, for addition of O_2, the system is not in the "high-pressure limit" where the association step is rate limiting. However, if these measurements are not in the high-pressure limit, it could only result in an increase in the magnitude of the actual microscopic rate constant. To verify that the rate constant for addition of CO to $Fe(CO)_4$ was not an anomaly, the addition reaction of another small ligand with a singlet ground state that is expected to lead to a product with a singlet ground state was also studied. H_2 reacts with $Fe(CO)_4$ under similar conditions as employed for the reaction of O_2 with $Fe(CO)_4$ with a rate constant of 1.9 (± 0.5) $\times 10^{-3}$ μs^{-1} $Torr^{-1}$ ($5.9 \pm 1.5 \times 10^{-14}$ cm^3 $molecule^{-1}$ s^{-1}), which is the same rate constant within experimental error as was measured for the reaction of $Fe(CO)_4$ + CO. The product of this reaction has absorptions that are consistent with formation of $H_2Fe(CO)_4$.[48,49]

It now seems reasonable to draw inferences regarding the spin states of the species observed in this study on the basis of the relative magnitudes of the rate constants for the various reactions that lead to formation and reaction of the species observed in this work. For example, the rapid formation of $Fe_2(CO)_7$ from the reaction of $Fe(CO)_2$ with $Fe(CO)_5$ is compatible with $Fe_2(CO)_7$ being formed in a triplet state. The rapid reaction of $Fe_2(CO)_7$ with CO to form the bridged isomer of $Fe_2(CO)_8$ would then be compatible with this isomer of $Fe_2(CO)_8$ being a triplet-state species. The unbridged isomer of $Fe_2(CO)_8$ is formed by a rapid reaction of $Fe(CO)_3$ and $Fe(CO)_5$, compatible with it too having a triplet ground state. It also reacts very slowly with CO to form $Fe_2(CO)_9$ with a rate constant that is 5 orders of magnitude smaller than gas kinetic. As with the slow reaction of $Fe(CO)_4$ + CO this process does not have a significant activation energy, implying that the spin-disallowed nature of the reaction is manifested in the preexponential. Reaction of the unbridged isomer of $Fe_2(CO)_8$ with $Fe(CO)_5$ has not been observed.

The spin states of Fe(CO) and $Fe_2(CO)_6$, are not known. However, the rapid reaction of Fe(CO) with $Fe(CO)_5$ to form $Fe_2(CO)_6$ implies they are likely to have the same spin state. The excited state of $Fe(CO)_3$, which is likely to be the first excited singlet state, is collisionally quenched to the ground state of $Fe(CO)_3$ with sufficient efficiency that we were not able to study reactions of this species with either CO or $Fe(CO)_5$. $Fe(CO)_4$*, which is expected to be a singlet-state species, reacts rapidly with $Fe(CO)_5$.

Finally, though some formally spin-forbidden reactions occur, it is interesting that neither $Fe_2(CO)_7$ nor the unbridged and bridged $Fe_2(CO)_8$ isomers demonstrate any tendency to react further with parent on the time scale of the present study. $Fe_2(CO)_7$ and unbridged $Fe_2(CO)_8$ reacted instead with the relatively insignificant amount of nascent CO present in the system. The reaction of unbridged $Fe_2(CO)_8$ + (nascent) CO, observed on a millisecond time scale with 351-nm photolysis of $Fe(CO)_5$, which is expected to be spin forbidden, occurred to the complete exclusion of trinuclear formation despite an $Fe(CO)_5$ concentration 30 times larger than that of the nascent CO. From these studies, it appears that though spin effects are an important predictive factor in determining the magnitude of a rate constant for reaction of coordinatively unsaturated metal carbonyls, they are not the only factor.

IV. Conclusions

The initial photoproducts formed on single-photon excimer laser photolysis of gas-phase $Fe(CO)_5$ and their subsequent reactions with CO and parent have been studied by transient infrared spectroscopy using a diode laser as the probe. The diode laser can be tuned to any arbitrary frequency. Thus, unlike a previous study[20] which used a CO laser, the presence of vibrationally excited CO, which by necessity absorbs CO laser radiation, does not mask underlying metal carbonyl absorptions. In addition, the diode laser affords a wider tuning range, which allowed for the direct probing of high-frequency CO absorptions belonging to polynuclear iron carbonyls formed on the reaction of coordinatively unsaturated iron carbonyls with parent.

A number of previously unknown species as well as species observed for the first time in the gas phase have been detected. The initial photoproducts of the 193-nm photolysis of $Fe(CO)_5$, $Fe(CO)_2$, and a species tentatively assigned to Fe(CO) were observed to react at near gas kinetic rates with parent to form species assigned as $Fe_2(CO)_7$ and $Fe_2(CO)_6$ (tentative), respectively. Further reaction of $Fe_2(CO)_7$ with the nascent CO produced on $Fe(CO)_5$ photolysis formed a dinuclear product whose absorptions were consistent with those of a doubly bridged $Fe_2(CO)_8$ isomer previously observed in matrix isolation studies.[36] The initial photoproducts formed on 248-nm photolysis of $Fe(CO)_5$, $Fe(CO)_2$, and $Fe(CO)_3$ behaved consistently with the species assigned to $Fe(CO)_2$ and $Fe(CO)_3$ in the 193- and 351-nm photolysis systems, respectively. $Fe(CO)_3$ and $Fe(CO)_4$, formed on 351-nm photolysis of $Fe(CO)_5$, reacted with parent to form the unbridged $Fe_2(CO)_8$ isomer, which also has been observed in a rare-gas matrix,[36] and $Fe_2(CO)_9$, respectively. The unbridged $Fe_2(CO)_8$ species reacted further with CO to form stable, triply bridged $Fe_2(CO)_9$.

Species best assigned as excited singlet states of $Fe(CO)_3$ and $Fe(CO)_4$ were observed to form as initial photoproducts following 351- and 248-nm photolysis, respectively. These species are rapidly collisionally quenched to their respective ground states but the rate of reaction of $Fe(CO)_4$* with $Fe(CO)_5$ was measured and has a magnitude compatible with that expected for a spin-allowed reaction.

The magnitudes of the rate constants for reaction of the coordinatively unsaturated metal carbonyls with parent $Fe(CO)_5$ or CO (summarized in Table I) are consistent with the expectation that spin-allowed reactions will be rapid while formally spin-disallowed reactions will be considerably slower. Further evidence that spin conservation affects reaction rates came from a comparison of the rate of reaction of $Fe(CO)_4 + O_2$ and $Fe(CO)_4$ + CO. The former reaction using O_2 was measured to be 50 times the rate observed for the reaction of $Fe(CO)_4$ + CO. The rate for reaction of $H_2 + Fe(CO)_4$, which is expected to be a spin-forbidden process, is virtually identical with the formally spin-forbidden reaction of $Fe(CO)_4$ + CO.

Acknowledgment. We acknowledge support of this work by the National Science Foundation under Grant NSF-88-06020. We also acknowledge partial support of this work by the donors of the Petroleum Research Fund, administered by the American Chemical Society under Grant 18303-AC6,3. We thank Prof. M. Poliakoff for a number of useful discussions and suggestions, which were made possible by NATO support under a collaborative grant.

(47) Berson, J. A. In *Diradicals*, Borden, T. W., Ed.; Wiley-Interscience: New York, 1982; Chapter 4.
(48) Hayes, D.; Weitz, E. *J. Phys. Chem.* **1991**, *95*, 2723.
(49) Miller, M. E.; Grant, E. R. *J. Am. Chem. Soc.* **1987**, *109*, 7951.